The Plant Cell, Vol. 24: 2733–2744, July 2012, www.plantcell.org

RESEARCH ARTICLES

Pod Corn Is Caused by Rearrangement at the *Tunicate1* Locus [W] [OA]

Jong-Jin Han,[a,b] David Jackson,[a] and Robert Martienssen[a,c,1]

[a] Cold Spring Harbor Laboratory, Cold Spring Harbor, New York 11724
[b] Molecular and Cellular Biology Graduate Program, Stony Brook University, Stony Brook, New York 11794
[c] Howard Hughes Medical Institute–Gordon and Betty Moore Foundation, Cold Spring Harbor Laboratory, Cold Spring Harbor, New York 11724

Pod corn (*Zea mays* var *tunicata*) was once regarded as ancestral to cultivated maize, and was prized by pre-Columbian cultures for its magical properties. *Tunicate1* (*Tu1*) is a dominant pod corn mutation in which kernels are completely enclosed in leaflike glumes. Here we show that *Tu1* encodes a MADS box transcription factor expressed in leaves whose 5′ regulatory region is fused by a 1.8-Mb chromosomal inversion to the 3′ region of a gene expressed in the inflorescence. Both genes are further duplicated, accounting for classical derivative alleles isolated by recombination, and *Tu1* transgenes interact with these derivative alleles in a dose-dependent manner. In young ear primordia, TU1 proteins are nuclearly localized in specific cells at the base of spikelet pair meristems. *Tu1* branch determination defects resemble those in *ramosa* mutants, which encode regulatory proteins expressed in these same cells, accounting for synergism in double mutants discovered almost 100 years ago. The *Tu1* rearrangement is not found in ancestral teosinte and arose after domestication of maize.

INTRODUCTION

Modern cultivated maize (*Zea mays*), unlike other grasses in the Poaceae, has a unique feature of severe reduction in glume size that results in almost naked grains. By contrast, pod corn (*Zea mays* var *tunicata*) kernels are entirely enclosed in long glumes, resembling most grasses, and for this reason, pod corn was widely regarded as a primitive form of cultivated maize (Mangelsdorf, 1947). Pod corn was first described in the 19th century as an ancient variety of maize that had been preserved by pre-Columbian cultures in Brazil (Saint-Hilaire, 1829), Mexico, and Peru. Later, prehistoric cobs excavated from San Marcos Cave, dated 5200 to 3400 B.C., were found to have relatively long glumes and were believed to possibly be a weak form of pod corn (Mangelsdorf et al., 1964). Genetic mapping revealed that pod corn was attributable to a single dominant gene, *Tunicate1* (*Tu1*) (Mangelsdorf and Galinat, 1964). *Tu1* behaved as a compound locus, such that rare recombinants gave rise to weak (*Tu1-l*) and intermediate (*Tu1-md*) alleles (Mangelsdorf and Galinat, 1964). A third derivative, *Tu1-d*, was phenotypically similar to *Tu1-l*, which led to the idea that weak alleles had one or two recombinable components, whereas *Tu1* had three components; in this way, doses could vary from one to six, and recombination could first dissect and then regenerate the full *Tu1* phenotype (Mangelsdorf and Galinat, 1964; Langdale et al., 1994). Derivatives were rare; therefore, the duplication of a recombinable component was considered as an explanation for the compound *Tu1* (Mangelsdorf and Galinat, 1964). The role of *Tu1* in the origin of maize was fraught with controversy (Mangelsdorf, 1947, 1984).

The *Tu1* phenotype is pleiotropic (Eyster, 1921; Nickerson and Dale, 1955; Langdale et al., 1994) and results in the conspicuous elongation of outer glumes, as well as sex reversal in the tassel and branching in the ear (Figure 1). *Tu1* genetically interacts with various morphological mutants that relate to juvenile-to-adult transition, such as *Corngrass1* (*Cg1*), *Teopod1* (*Tp1*), and *Tp2*, branching, such as *ramosa1* (*ra1*), and sex determination, such as the *tassel seed* mutants *ts1*, *ts2*, *ts4*, *Ts5*, and *Ts6* (Collins, 1917; Langdale et al., 1994). Based on these genetic studies, *Tu1* has been proposed to play roles in phase transition, branch meristem formation, spikelet initiation, and sex determination. Despite robust genetic and morphological studies, the molecular function of *Tu1* in a diverse range of floral developmental processes is largely unknown, as is the nature of genetic modification that leads to the *Tu1* phenotype.

MADS box genes in plants are well known for regulating floral organ identity as well as developmental phase transition (Hartmann et al., 2000; Ng and Yanofsky, 2001; Yu et al., 2002; Whipple et al., 2004). A MADS box gene in maize, *Z. mays* MADS19 (*Zmm19*), lies in the same genetic interval as *Tu1* (Münster et al., 2002; He et al., 2004). Furthermore, ectopic expression of *Zmm19* results in leaflike sepals in *Arabidopsis thaliana*, resembling the elongated glumes in *Tu1* mutants (He et al., 2004; Wingen et al., 2012). *Zmm19* is misexpressed in the inflorescence of *Tu1* mutants, and two duplicated copies of the gene were found in *Tu1*, but only one copy was found in *Tu1-l*, *Tu1-d*, and *Tu1-md* (He et al., 2004; Wingen et al., 2012). Despite these promising indications, genome sequencing has

[1] Address correspondence to martiens@cshl.edu.
The author responsible for distribution of materials integral to the findings presented in this article in accordance with the policy described in the Instructions for Authors (www.plantcell.org) is: Robert Martienssen (martiens@cshl.edu).
[W] Online version contains Web-only data.
[OA] Open Access articles can be viewed online without a subscription.
www.plantcell.org/cgi/doi/10.1105/tpc.112.100537

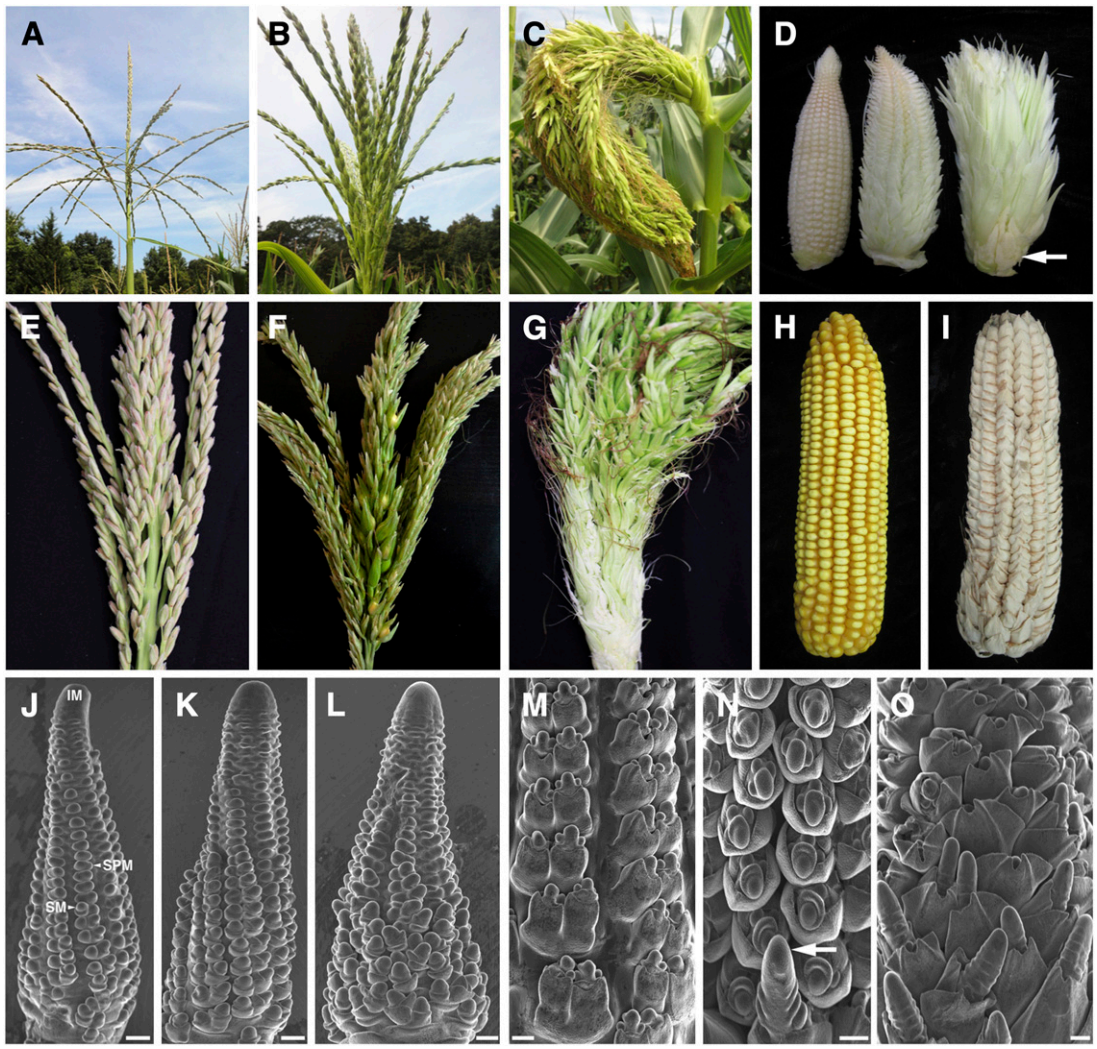

Figure 1. *Tu1* Mutant Phenotypes.

(A) and **(E)** Mature tassel phenotype of wild-type plants.
(B) and **(F)** Mature heterozygous *Tu1* tassel with partially elongated and feminized florets. Feminized florets with silk produced kernels via successful fertilization **(F)**.
(C) and **(G)** Mature homozygous *Tu1* tassel with fully elongated and feminized florets. Single silk strands emerged from the feminized spikelets in *Tu1* homozygous tassels.
(D) Unfertilized ears of wild-type (left), heterozygous *Tu1* (middle), and homozygous *Tu1* (right). Heterozygous *Tu1* ear displayed elongated glumes in comparison with the wild type. Further elongated glumes and abnormal branches (arrow) were observed in homozygous *Tu1* ear.
(H) Mature kernels were naked in the wild-type ear.
(I) The presence of elongated glumes made kernels invisible in the mature heterozygous *Tu1* ear.
(J) to **(L)** Scanning electron micrographs of 2-mm-long ear development of the wild type **(J)**, heterozygous *Tu1* mutant **(K)**, and homozygous *Tu1* mutant **(L)** with irregular seed rows.
(M) to **(O)** Scanning electron micrographs of 4-mm-long ear development. SMs in the wild type converted into a pair of FMs surrounded by glumes **(M)**. Heterozygous *Tu1* mutants also produced FMs normally except for a few cases of an indeterminate branch (arrow) **(N)**. However, homozygous *Tu1* mutants showed failure of FM conversion and instead formed indeterminate branches with largely elongated glumes at the base of the ear **(O)**.
Bars in **(J)** to **(O)** = 0.2 mm.

revealed several other candidate genes in the same interval (Schnable et al., 2009). For example, *miR172c* is found in this same genetic interval on chromosome 4 (Wei et al., 2009), and double mutants between *Tu1* and *miR172e/ts4* (Chuck et al., 2007b) are strongly synergistic (Langdale et al., 1994) with respect to both branching and sex determination. Also, *Tu1* has a synergistic interaction with *Cg1*, which encodes two *miR156* genes, *miR156b* and *miR156c* (Langdale et al., 1994; Chuck et al., 2007a). *miR156* shows antagonistic interactions with *miR172*, which, similar to MADS box genes, has regulatory roles

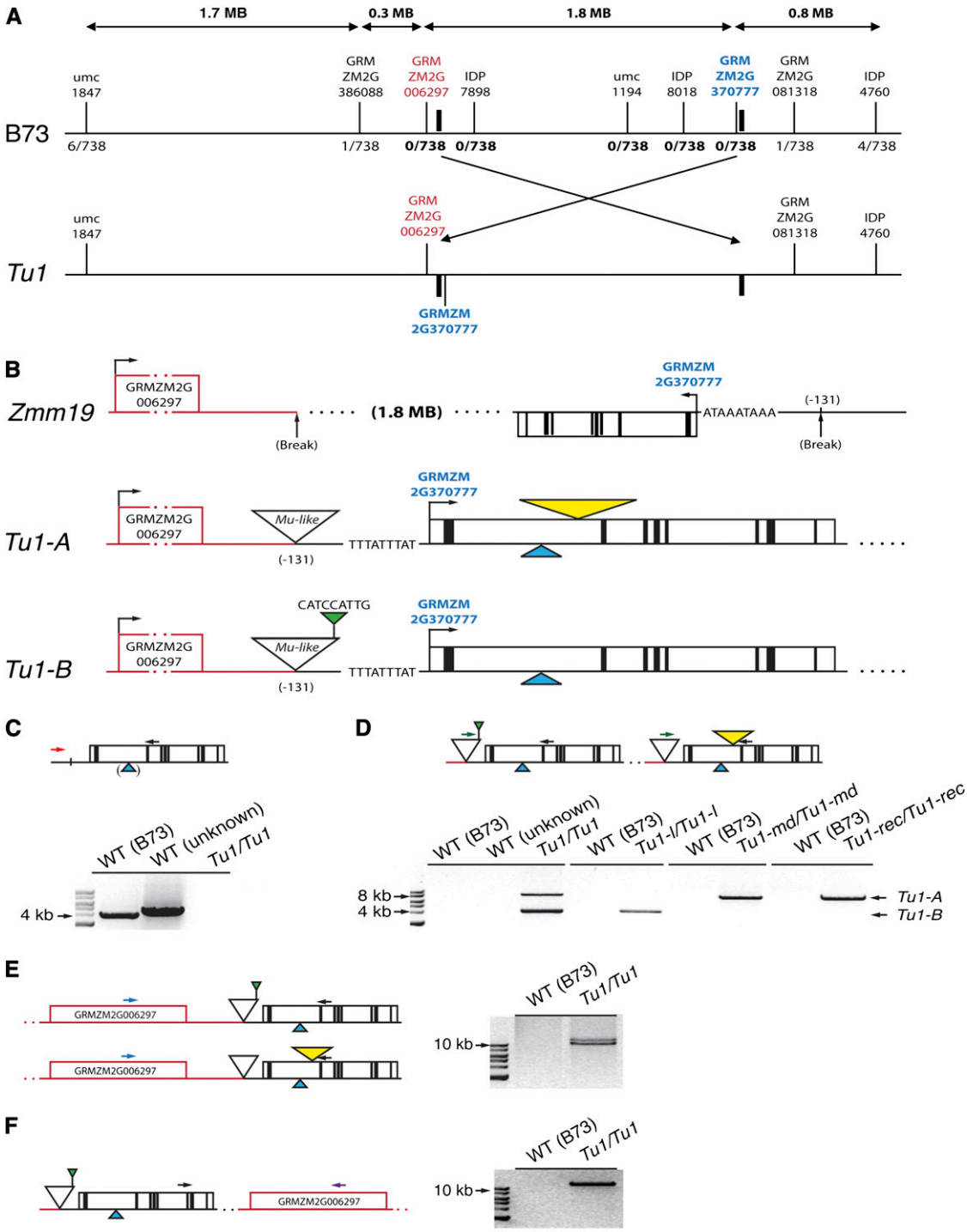

Figure 2. Rearrangement of *Tu1*.

(A) Genetic map of the *Tu1* locus with genetic markers. Recombination frequency is indicated by number of recombinants over total population size, with a recombination cold spot proximal to *Tu1*.

(B) Schematic representation of *Tu1-A* and *Tu1-B* loci that are distinct from wild-type *Zmm19*, which is GRMZM2G370777. An unknown gene (GRMZM2G006297, red line), is located 1.8 Mb from *Zmm19* in the wild type but adjacent to both *Tu1-A* and *Tu1-B* in *Tu1*. A 3.5-kb insertion (yellow triangle) specific to *Tu1-A*, a 9-bp insertion (green triangle) specific to *Tu1-B*, and a novel *Mutator-like* insertion found in both *Tu1-A* and *Tu1-B* were absent from B73. *Zmm19* is represented by a box, and internal lines denote exons.

in the transition from vegetative to reproductive growth and in specifying floral organ identity by targeting genes involved in floral determinacy (Aukerman and Sakai, 2003; Chen, 2004; Chuck et al., 2007a; Zhu and Helliwell, 2011). The extent of the duplication in *Tu1* was not known; therefore, the possibility that one of these other candidates was responsible for the phenotype could not be eliminated.

Here, we describe phenotypic characteristics of *Tu1* and demonstrate that the *Tu1* locus is interrupted by a chromosomal rearrangement in the 5′ regulatory region of *Zmm19*. Our results indicate that the duplicate copies of *Zmm19* in *Tu1* are ~30 kb apart and that they can be recombined to result in a single copy with reduced phenotypic effects. At least one other gene is included in the duplication, but *Tu1* phenotypes are reconstituted in *Zmm19* transgenic plants when the rearranged locus is used to drive expression. TU1 protein fusions show a discrete expression pattern comparable to that of *ramosa* genes during an early stage of inflorescence development that reflects fusion of the promoter via a large chromosomal inversion to a gene expressed in the inflorescence. Based on its expression pattern and on these dose-dependent phenotypes, we suggest that *Tu1* is involved in inflorescence architecture by promoting indeterminate cell fate.

RESULTS

Tu1 Mutant Phenotypes Are Dose-Dependent

Tu1 was introgressed into the B73 background to examine its phenotype. Normal monoecious maize bears a distinct terminal male inflorescence, the tassel (Figures 1A and 1E), and a lateral female inflorescence, the ear (Figures 1D and 1H). *Tu1* is a dominant mutation; therefore, plants heterozygous for *Tu1* displayed pleiotropic defects in reproductive development, and plants homozygous for *Tu1* became even more severe in a dose-dependent manner. Both tassels and ears of *Tu1* mutants are associated with a spikelet formation defect in which outer glumes enclosing inner whorls are highly elongated in comparison with the wild type (Figures 1A to 1I). In heterozygous *Tu1*, elongated glumes were conspicuous at the base of the central rachis and lateral branches and became less prominent toward the inflorescence apex (Figures 1B and 1F), whereas homozygous *Tu1* tassels produced very large glumes (Figures 1C and 1G). In the wild type, bisexual floral meristems (FMs) of maize convert into unisexual flowers by a process of selective abortion of pistil primodia within the tassel and stamen primordia within the ear (Le Roux and Kellogg, 1999). In heterozygous *Tu1* tassels, pistils failed to abort. Male flowers were partially converted into female flowers near the base, and some bore kernels after fertilization (Figures 1B and 1F). This feminization was more prominent in homozygous *Tu1* (Figures 1C and 1G).

Unlike the naked kernels found in the wild type (Figure 1H), kernels in heterozygous *Tu1* were fully enclosed by glumes (Figure 1I). After removing leaflike glumes, several long branches, which are normally found only in the tassel, were found in homozygous *Tu1* ears (Figure 1D, arrow). Using scanning electron microscopy of 2-mm developing ears, we observed the inflorescence meristem (IM), spikelet pair meristem (SPM), and spikelet meristem (SM) with bract growth in the wild type (Figure 1J). Figure 1L shows the irregular rows of the SM from homozygous *Tu1* inflorescences, which are very different from the regular pattern of the organized SM on the flanks of the wild-type ear tip (Figure 1J). When ears become ~4 mm long, the two SMs, generated from each SPM, convert into FMs that initiate floral organs, including anthers and pistil primordia (Figure 1M). Heterozygous *Tu1* ears mostly succeeded in FM conversion from SM, only producing an indeterminate branch rarely (Figure 1N, arrow). However, despite the obvious glume elongation in homozygous *Tu1*, we could observe numerous indeterminate long branches emerging as a consequence of failure in FM transition (Figure 1O), suggesting that the *Tu1* ear adopts features of the male inflorescence (Bortiri and Hake, 2007). These phenotypes suggest that *Tu1* mutants have defects in suppressing glume formation and in meristem fate and sex determinacy.

Fine Mapping of *Tu1*

The *Tu1* mutation was mapped to the long arm of chromosome 4 (Mangelsdorf and Galinat, 1964). We set out to fine map the *Tu1* locus by backcrossing *Tu1* heterozygotes (*Tu1*/+) to wild-type plants twice. We screened 738 F2 plants using markers from the region, and *Tu1* was subsequently delimited between one cleaved-amplified polymorphic sequence (CAPS) marker for GRMZM2G386088 and one Insertion/Deletion (InDel) marker for

Figure 2. (continued).

(C) Schematic representation of wild-type *Zmm19* with 293-bp insertion (blue triangle) in first intron, which is absent in B73 but present in unknown wild-type (WT) *tu1* background. Allele-specific PCR showing that 5′ upstream region of wild-type *Zmm19* is absent from *Tu1*. The positions of primers are depicted as arrows. Red arrow specific to 5′ upstream region of wild-type *Zmm19*.

(D) PCR verification of *Tu1* locus. Although duplicated *Tu1-A* and *Tu1-B* loci are found in *Tu1*, half-tunicate mutants, which are *Tu1-l* and *Tu1-md*, respectively, possess one copy of duplicated *Tu1* loci. New *Tu1* derivative allele, *Tu1-rec*, was detected in our mapping population (one out of 738) and bears only the *Tu1-A* but not *Tu1-B*. The position of primers is depicted as arrows. Green arrow specific to *Mutator-like* insertion, which is present only in *Tu1* alleles.

(E) Both duplicated *Tu1-A* and *Tu1-B* loci have an unknown gene (GRMZM2G006297) as their 5′ upstream gene. Two amplicons are the product of two recombined genes between *Zmm19* and the unknown gene. Blue arrow specific to GRMZM2G006297. Although forward primers were uniquely designed for allele-specific PCRs, the same reverse primer (black arrow) was used as in **(C)**.

(F) Duplicated *Tu1-A* and *Tu1-B* loci neighbor each other. GRMZM2G006297 is located at the 3′ downstream region of *Tu1-B* and at the 5′ upstream region of *Tu1-A* (Figure 2E; see Supplemental Figure 2 online). Purple arrow specific to GRMZM2G006297. Gel images were inverted for better contrast, and New England BioLabs 1 kb DNA ladder was used [**(C)** to **(F)**].

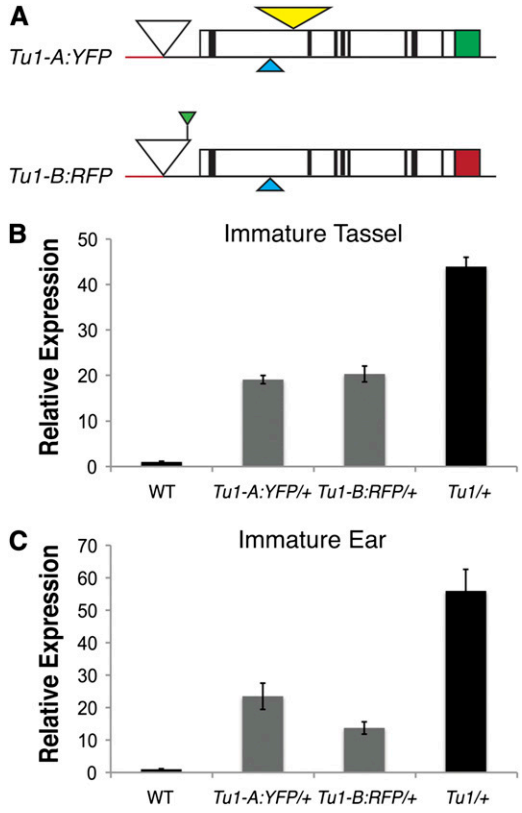

Figure 3. *Zmm19* Expression Level of *Tu1-A*:*YFP* and *Tu1-B*:*RFP* Transgenic Lines Is Correlated with Copy Number.

(A) Structure of *Tu1-A*:*YFP* and *Tu1-B*:*RFP* constructs. Both the 700 bp of the 3′ downstream region of GRMZM2G006297 (red line) and the 2-kb novel *Mu-like* element (white triangle) were cloned with the reporter gene, *YFP* (green box) and *RFP* (red box), into the *Tu1-A* and *Tu1-B* allele and the endogenous promoter region.

(B) The immature tassels of *Tu1-A*:*YFP* and *Tu1-B*:*RFP* transgenic lines showed one-half the expression level of *Zmm19* compared with heterozygous *Tu1* immature tassel (*Tu1*/+, black bar), which was used as a reference. qRT-PCR of two biological replicates. See also Supplemental Figure 3A online. WT, wild type.

(C) The immature ears of *Tu1-A*:*YFP* and *Tu1-B*:*RFP* transgenic lines also showed one-half the expression level of heterozygous *Tu1* immature ears (*Tu1*/+, black bar). qRT-PCR of three biological replicates. See also Supplemental Figure 3B online. Results are plotted as the ratio to the wild-type level of *Zmm19* and are represented as mean ± SE. *Zmm19 is* normalized to *Ubiquitin* levels. *Tu1-A*:*YFP*/+ and *Tu1-B*:*RFP*/+ indicate heterozygous *Tu1-A*:*YFP* and heterozygous *Tu1-B*:*RFP* plants, respectively.

GRMZM2G081318, with only one recombinant each, covering a 2.5-Mb interval. To further narrow down the interval, we used two InDel markers, two insertion-deletion polymorphism (IDP) markers, and one simple sequence repeat (SSR) marker. Interestingly, these five genetic markers showed no recombination within a 1.8-Mb interval, revealing a recombination cold spot proximal to *Zmm19* that did not recombine with *Tu1* (Figure 2A). Sequencing of BAC clones in a 22-Mb interval surrounding *Zmm19* (Wei et al., 2009) allowed comparative DNA sequence analyses between the *Zmm19* gene copies found in *Tu1*, known as *Tu1-A* (GenBank number AJ850302) and *Tu1-B* (GenBank number AJ850303), and the *Zmm19* copy found in the reference sequence of the B73 genome. This analysis revealed that both *Tu1-A* and *Tu1-B* are structurally rearranged by insertion of a novel 2-kb *Mu-like* element in the 5′ *cis*-regulatory region of *Zmm19*, which is fused with the 3′ flanking region of an unknown gene (GRMZM2G006297) located on the other side of the 1.8-Mb interval from *Zmm19* in the opposite orientation (Figure 2B).

This 1.8-Mb chromosomal inversion would be expected to inhibit recombination and likely accounts for the cold spot (Figure 2A) that prohibited previous attempts to precisely map *Zmm19* relative to *Tu1* (Münster et al., 2002; He et al., 2004; Wingen et al., 2012). The analyses also revealed that *Tu1-A* is distinguished from *Tu1-B* by the presence of a 3.5-kb insertion in the first intron, a non–long terminal repeat retrotransposon (Figure 2B, yellow triangle). Allele-specific PCR confirmed that the wild type has a single copy of *Zmm19* (Figure 2C), whereas *Tu1* has both *Tu1-A* and *Tu1-B* (Figures 2D and 2E). Additional comparative sequence analyses and PCR showed that half-tunicate mutants, *Tu1-l* and *Tu1-md*, have only one copy of *Tu1-B* or *Tu1-A*, respectively (Figure 2D). Finally, in one rare recombinant out of 738, we observed de novo crossover between *Tu1-A* and *Tu1-B* (*Tu1-rec*, Figure 2D), reconstructing the half-tunicate phenotype (see Supplemental Figure 1B online) as previously reported (Mangelsdorf and Galinat, 1964). The primer pairs used in Figure 2E are separated by 1.8 Mb; therefore, only recombined *Tu1* alleles can be amplified but not the wild type. Long-range PCR and sequencing revealed that *Tu1-B* is positioned upstream of *Tu1-A*, and the intervening 30-kb DNA sequence includes *gypsy-like* and *copia-like* retrotransposons, *dSpm-like* and *hAT-type* DNA transposons, and another copy of GRMZM2G006297 fused with the promoter region of *Tu1-A*, indicating that GRMZM2G006297 is contained within the duplication (Figures 2E and 2F; see Supplemental Figure 2 online). We conclude that inversion preceded duplication at the *Tu1* locus and that GRMZM2G006297 and *Zmm19* are both strong candidate genes for *Tu1* and cannot be further distinguished by recombination.

Zmm19 Transgenic Lines Phenocopy *Tu1*

We used transgenic plants to determine whether the *Tu1* phenotype was caused by the rearrangement at *Zmm19*. We fused *Tu1-A* with yellow fluorescent protein (YFP) and *Tu1-B* with red fluorescent protein (RFP) at their C termini (Figure 3A) and generated several independent transgenic maize plants with each transgene (see Methods). Each transgene was driven by its own promoter, which comprised 3 kb of upstream sequence, including the 3′ flanking region of GRMZM2G006297 and the 2-kb *Mu-like* transposon. Maize plants were transformed individually with these two constructs (*Tu1-A*:*YFP* and *Tu1-B*:*RFP*) and were backcrossed to B73. We performed quantitative RT-PCR (qRT-PCR) analysis with RNA from immature tassel and ear. Each single transformant showed a significant increase in the *Zmm19* transcript abundance in both tissue types, but the relative expression level was about one-half of the transcript level of heterozygous *Tu1* (*Tu1*/+), which possesses both *Tu1-A* and *Tu1-B* (Figures 3B and 3C). Homozygous *Tu1* (*Tu1*/*Tu1*)

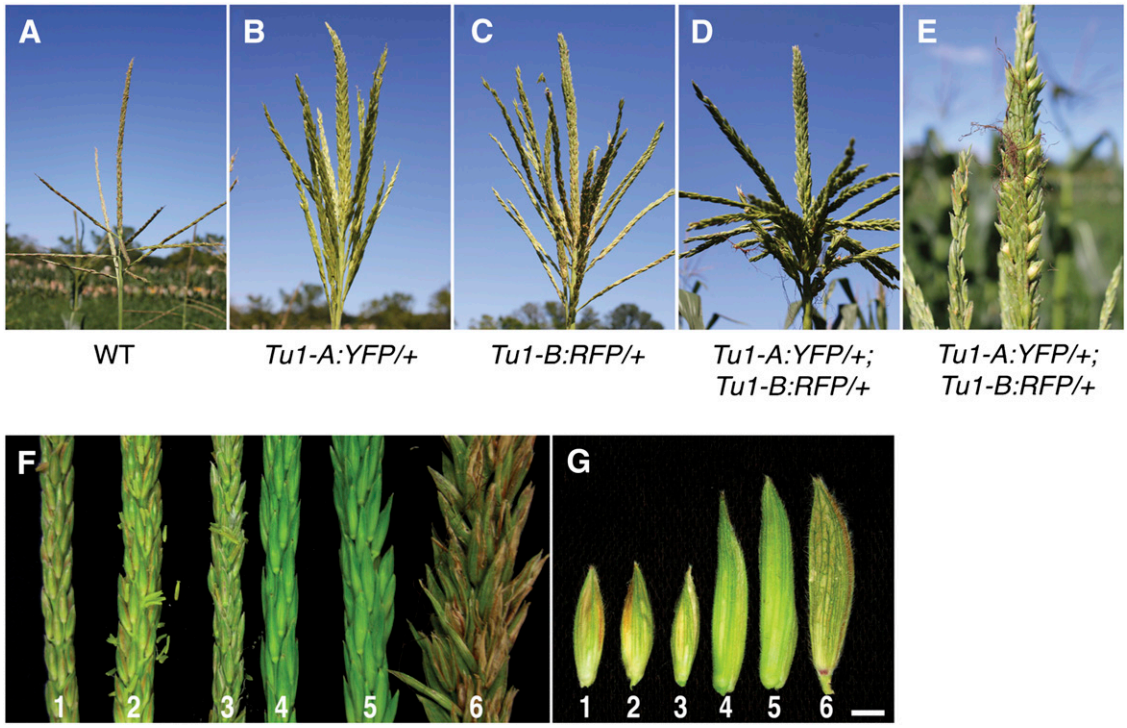

Figure 4. *Tu1-A*:*YFP* and *Tu1-B*:*RFP* Transgenic Plants Resemble the *Tu1* Tassel Phenotype.

(A) Wild-type (WT) tassel.
(B) and **(C)** Single transgenic tassels heterozygous for *Tu1-A*:*YFP* **(B)** and *Tu1-B*:*RFP* **(C)** had a rachis and lateral branches, respectively, that were relatively thicker than those of the wild-type tassel **(A)** because of elongated glumes.
(D) and **(E)** Transgenic plants harboring two transgenes (*Tu1-A*:*YFP* and *Tu1-B*:*RFP*) showed dense spikelets with elongated glumes **(D)** and successful kernel-bearing fertilization **(E)** in the tassel.
(F) and **(G)** *Tu1-A*:*YFP* and *Tu1-B*:*RFP* transgenic plants showed elongated glume phenotypes that are distinct from those of wild-type plants. Morphological change was detected in a single glume phenotype of the transgenic plants **(G)**, which is comparable to heterozygous *Tu1* plants. 1, B73; 2, Mo17; 3, transgenic control (wild type), 4, heterozygous *Tu1-A*:*YFP* (*Tu1-A*:*YFP* /+); 5, heterozygous *Tu1-B*:*RFP* (*Tu1-B*:*RFP*/+); 6, heterozygous *Tu1* (*Tu1*/+).
Bar in **(G)** = 2.5 mm.

further doubled *Zmm19* transcript abundance compared with heterozygous *Tu1* (*Tu1*/+) (see Supplemental Figures 3A and 3B online). Expression of the transgene in transgenic immature tassels and ears was weaker than that observed in *Tu1*/+ heterozygotes, but was much higher than in wild-type inbreds. These data suggest that *Zmm19* ectopic expression levels in inflorescences are correlated with *Tu1* copy number.

Tu1-A:*YFP* and *Tu1-B*:*RFP* T1 transgenic plants produced elongated glumes in the tassel (Figures 4F and 4G) and were stable after backcrossing to B73 (Figures 4B and 4C). We tested the additive effect of the two transgenes by crossing *Tu1-A*:*YFP* and *Tu1-B*:*RFP* transgenic lines. Plants carrying both *Tu1-A*:*YFP* and *Tu1-B*:*RFP* had further elongated glumes (Figure 4D) and occasional feminization that enables spikelets to bear seed in the tassel (Figure 4E), resembling *Tu1*/+ heterozygotes (Figure 1F). Elongated glumes in plants with both transgenes led the main rachis and lateral branches to seem thicker than those in single transgenic and nontransgenic plants, suggesting that both transgenes are functionally involved in the *Tu1* tassel phenotype (Figure 4D; see Supplemental Figures 4A to 4F online). Similarly, tassel phenotypes were more conspicuous when transgenic lines were combined with *Tu1-l*, suggesting that both transgenes interact with *Tu1-l* in a dose-dependent manner (Figures 5A to 5G). We observed that *Tu1-A*:*YFP* and *Tu1-B*:*RFP* transgenic plants exhibited weak half-tunicate ear phenotypes, resembling those of *Tu1-l* single-copy derivatives (Figures 6A and 6B). Plants with both transgenes produced glumes that fully covered every kernel (Figure 6A) and were comparable to *Tu1*/+ heterozygotes (Figure 1I). Furthermore, crosses between *Tu1-A*:*YFP* or *Tu1-B*:*RFP* and *Tu1-l* resulted in a dramatic enhancement of the half-tunicate phenotype in the ear (Figure 6B), indicating that the transgenes complemented half-tunicate derivatives and provided *Tu1* function (Mangelsdorf and Galinat, 1964). Thus, our data demonstrate that ectopic expression of *Zmm19* derived from the *Tu1* locus causes the dose-dependent *Tu1* phenotype.

Nuclear Localization of TU1-A:YFP and TU1-B:RFP Proteins

Zmm19 contains a highly conserved DNA binding MADS box domain and is therefore expected to be nuclear-localized (Ng and Yanofsky, 2001; Münster et al., 2002). Confocal imaging

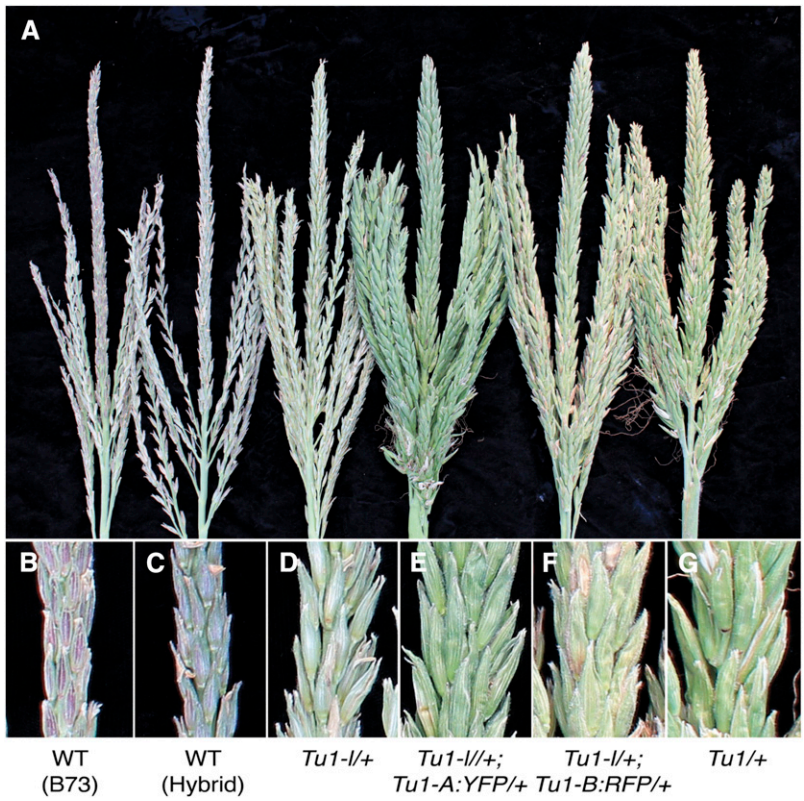

Figure 5. *Tu1-A*:*YFP* and *Tu1-B*:*RFP* Transgenic Lines Interact with *Tu1-I*.

(A) Each single transgenic line produced an additive tassel phenotype with the presence of the *Tu1-I* allele compared with a single *Tu1-I*. The order of each tassel in **(A)** corresponds with those in **(B)** to **(G)**.

(B) to **(G)** A close-up view of **(A)**, showing that glumes were elongated in a dose-dependent manner. Rachis phenotype of B73 wild-type (WT) inbred **(B)**, hybrid between B73 and the wild-type transformant **(C)**, a single-copy *Tu1-I* heterozygote **(D)**, double heterozygote for *Tu1-I* and *Tu1-A*:*YFP* **(E)**, double heterozygote for *Tu1-I* and *Tu1-B*:*RFP* **(F)**, and *Tu1* heterozygote **(G)**.

revealed that TU1-A:YFP and TU1-B:RFP accumulated in nuclei of mature leaf and glume epidermis, as expected (Figures 7A to 7D). We further examined *Tu1-A*:*YFP* lines to investigate the expression of TU1 in different cell types. Nuclear localization was detected not only in vegetative tissues, mature leaves, and husks, but also in glumes, trichomes, and FMs (Figure 7; see Supplemental Figure 5 online). Colocalization of the two fusion proteins was consistent with their overlapping function (see Supplemental Figures 6A and 6B online). Expression of the fluorescent protein–tagged proteins in vegetative tissues was expected based on the transcription pattern of *Zmm19* (GRMZM2G370777) in wild-type plants (see Supplemental Figure 7A online). However, *Zmm19* was ectopically expressed in the early inflorescence of *Tu1* (Figure 3; see Supplemental Figure 3 online), and the fusion proteins persisted in even later developmental stages, when tassel glumes were fully developed with trichomes (Figures 7B and 7D; and Supplemental Figure 5B online).

In the maize inflorescence, meristem determinacy is progressively restricted, such that tertiary SMs arise from the secondary SPMs, which in turn arise from the primary IM (Vollbrecht et al., 2005). Whereas the spikelet pair is considered a short branch, long branches resemble the primary inflorescence and are normally found only at the base of the tassel. In homozygous *Tu1*/*Tu1* mutants, long branches also arose at the base of the ear (Figures 1D and 1O), resembling *ramosa* mutants in this respect (Vollbrecht et al., 2005; Bortiri et al., 2006; Satoh-Nagasawa et al., 2006). Both functional TU1 fusion proteins were expressed in a small cup-shaped subset of cells at the base of the SPM in young ear primordia (Figures 8A and 8B). Remarkably, this expression pattern is similar to that of the short-branch determination genes, *Ramosa1* (*Ra1*) and *Ra3*, in wild-type plants (Vollbrecht et al., 2005; Bortiri et al., 2006; Satoh-Nagasawa et al., 2006). Imaging of a double transgenic plant revealed that the YFP and RFP fusion proteins were co-localized to the nuclei in this domain (Figure 8C). These images suggest that ectopic expression of TU1/ ZMM19 at the base of developing SMs promotes their abnormal indeterminacy.

DISCUSSION

We have found that the pod corn mutant *Tu1* is caused by the ectopic expression of the MADS box gene *Zmm19* in the developing maize inflorescence. *Zmm19* is normally expressed

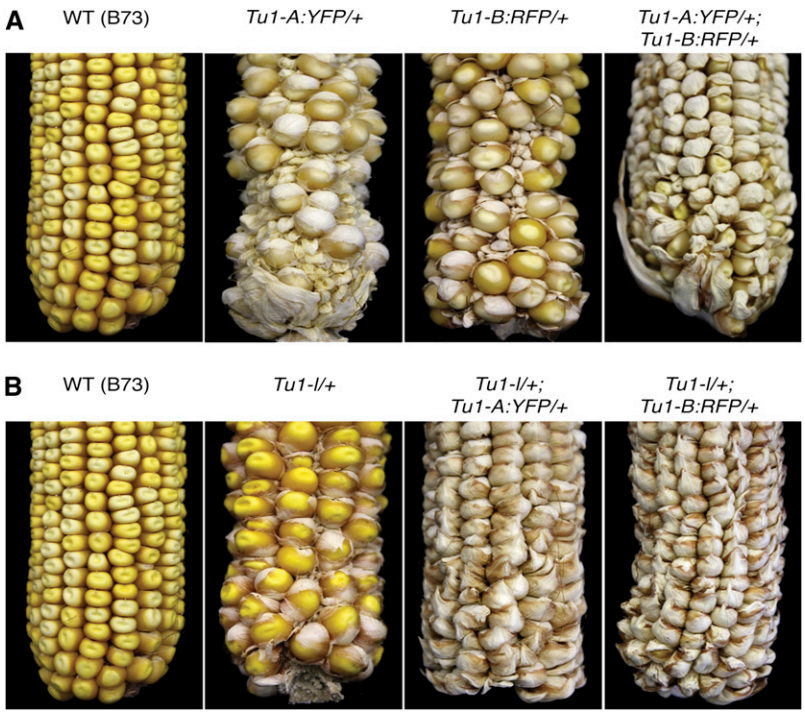

Figure 6. *Tu1-A*:*YFP* and *Tu1-B*:*RFP* Transgenic Ears Phenocopy *Tu1*.

(A) The half-tunicate phenotype was observed in transgenic ears carrying each single transgene (*Tu1-A*:*YFP*/+ or *Tu1-B*:*RFP*/+), whereas the wild-type (WT) kernels were naked. Two transgenes present in one transgenic line (*Tu1-A*:*YFP*/+; *Tu1-B*:*RFP*/+) caused glumes to be further elongated to fully enclose kernels, suggesting the additive genetic effect of the two transgenes.

(B) A single transgenic line (*Tu1-A*:*YFP*/+ or *Tu1-B*:*RFP*/+) produced fully elongated glumes with the presence of *Tu1-I*, whereas plants heterozygous for a single copy of *Tu1-I* (*Tu1-I*/+) represented the half-tunicate phenotype that was comparable to either the *Tu1-A*:*YFP*/+ or *Tu1-B*:*RFP*/+ phenotype **(A)**.

in husk and leaf tissues in the wild type (see Supplemental Figure 7A online) but is ectopically expressed in the inflorescence in *Tu1* because of a chromosomal rearrangement (see Supplemental Figure 3 online), most likely a large inversion associated with the transposition of a *Mutator-like* transposon. This rearrangement led to a mild half-tunicate phenotype, in which glumes extend but fail to enclose the kernel. Subsequently, duplication of the two genes at the breakpoint of this rearrangement enhanced the phenotype so that glumes completely covered the kernels. *Zmm19* has previously been proposed as a strong candidate gene to account for the *Tu1* phenotype, but definitive proof was lacking because of the nature of the chromosomal rearrangement, which prohibited fine mapping. We have shown that half-tunicate phenotypes can be phenocopied by *Tu1* transgenes and that these transgenes can interact with half-tunicate derivative alleles to reconstitute the full *Tu1*/pod corn phenotype.

The half-tunicate derivative alleles, *Tu1-I*, *Tu1-d*, and *Tu1-md*, were recovered by Mangelsdorf and Galinat after rare crossovers within the *Tu1* locus, and Mangelsdorf and Galinat reported that they could reconstitute *Tu1* by recombining *Tu1-I* and *Tu1-d*, suggesting that *Tu1* was a compound locus (Mangelsdorf and Galinat, 1964). They continued to characterize the half-tunicate phenotypes of *Tu1-I* and *Tu1-d* through repeated backcrossing to an inbred line and observed that *Tu1-d* consistently had longer glumes than *Tu1-I* in tassels and ears. Although the origin of *Tu1-md* is unclear, the phenotype of *Tu1-md* (see Supplemental Figure 1A online) is more severe than that of *Tu1-I* (Figure 6B), and this may be the stronger half-tunicate allele reported by Mangelsdorf and Galinat (1964) (Langdale et al., 1994).

Previously, genomic cloning recovered two *Zmm19* genes in *Tu1*, known as *Tu1-A* and *Tu1-B*, and one gene each in *Tu1-d*, *Tu1-I*, and *Tu1-md* (Munster et al., 2004; Wingen et al., 2012). Sequence analysis indicated that both *Tu1-I* and *Tu1-d* were analogous to *Tu1-B*, whereas *Tu1-md* was analogous to *Tu1-A*. We used PCR assays to confirm this organization and to reveal that the *Tu1-A* and *Tu1-B* genes were part of a larger 30-kb tandem duplication in *Tu1* that included at least one other gene (Figures 2D to 2F; see Supplemental Figure 2 online). It is plausible that the derivative alleles were caused by unequal crossover within this duplication, and indeed we recovered a derivative allele *Tu1-rec* among our *Tu1* mapping population at a frequency of one in 738, which is comparable to the one in 1300 frequency reported previously (Mangelsdorf and Galinat, 1964). The phenotype of *Tu1-rec* is comparable to that of *Tu1-md* (see Supplemental Figure 1 online) and is stronger than *Tu1-I* (Figure 6B), consistent with *Tu1-md* and *Tu1-rec* retaining *Tu1-A*, whereas *Tu1-I* retains *Tu1-B* (Figure 2D). We did not attempt to reconstitute the full tunicate phenotype from these

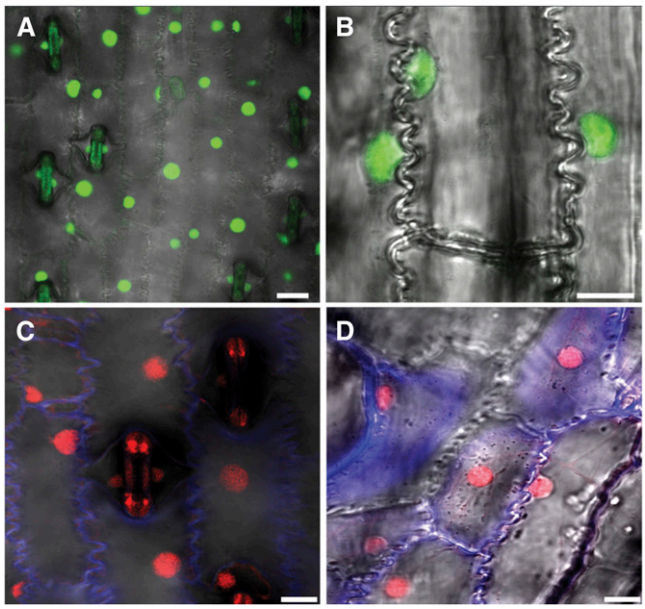

Figure 7. TU1-A:YFP and TU1-B:RFP Are Nuclear-Localized.

(A) and **(B)** TU1-A:YFP fusion proteins are nuclear-localized in leaf **(A)** and glume **(B)** epidermis.
(C) and **(D)** TU1-B:RFP fusion proteins are nuclear-localized in leaf **(C)** and glume **(D)** epidermis. Autofluorescence of YFP and RFP was detected from guard cells in the leaf epidermis **(A)** and **(C)**.
Bar in **(A)** = 20 μm; bars in **(B)** to **(D)** = 10 μm.

derivative alleles (Mangelsdorf and Galinat, 1964), given that they only have one and not two components as previously proposed (Langdale et al., 1994) and that the mechanism of reconstitution therefore remains unclear.

By comparison with the finished sequence of 22 Mb surrounding *Zmm19* in the B73 inbred line, we detected a large chromosomal inversion in *Tu1* whose breakpoint lies in the promoter region of *Zmm19*. This breakpoint results in fusion with the 3′ flanking region of an unknown gene, GRMZM2G006297. This unknown gene is duplicated along with *Zmm19* and is expressed in both husk leaves and inflorescences, unlike *Zmm19*, which is normally expressed in husk leaves (see Supplemental Figures 7A and 7B online). We considered three possibilities to explain why *Zmm19* expression is drastically altered in *Tu1*. First, a novel *Mu-like* element located at the breakpoint of the inversion may enhance *Zmm19* expression. However, we did not detect transcription start sites within the *Mu-like* element by 5′ RACE. Second, chromosomal inversion in the promoter of *Zmm19* may cause removal of enhancer-blocking insulators or silencers to upregulate *Tu1*. However, transgenic fusion proteins that contained these sequences were expressed in a specific subset of cells, making this possibility unlikely. Finally, *Zmm19* may adopt the expression pattern of the upstream gene GRMZM2G006297, accounting for ectopic expression in the male and female inflorescence.

In the wild type, RNA sequencing expression data revealed that *Zmm19* expression decreases during early tassel development (comparing samples taken at a tassel length of 1 to 2 mm with those at 5 to 7 mm), whereas GRMZM2G006297 expression increases. During the developmental progression from IM to FM, GRMZM2G006297 expression is upregulated in young ear primodia, where *Zmm19* is not normally expressed (A. Eveland, A. Goldshmidt, and D. Jackson, unpublished data). Thus, this upstream gene may be the cause of the cup-shaped expression pattern of TU1 fusion proteins, which typically resembles that of *ramosa* genes in young ear primodia. Interestingly, KNOTTED-1 (KN1) chromatin immunoprecipitation sequencing data (Bolduc et al., 2012) revealed that KN1 strongly binds this 3′ flanking region of GRMZM2G006297, which is fused with the *Zmm19* promoter by the *Tu1* rearrangement. KN1 targets genes in the gibberellin and brassinosteroid pathways, which are involved in sex determination in maize (Bolduc and Hake, 2009; Hartwig et al., 2011; Bolduc et al., 2012). Thus, it is possible that the ectopic expression of *Zmm19* may be associated with the *Kn1* gene network.

SHORT VEGETATIVE PHASE (*SVP*) is the closest homolog of *Zmm19* in *Arabidopsis* and regulates flowering repression

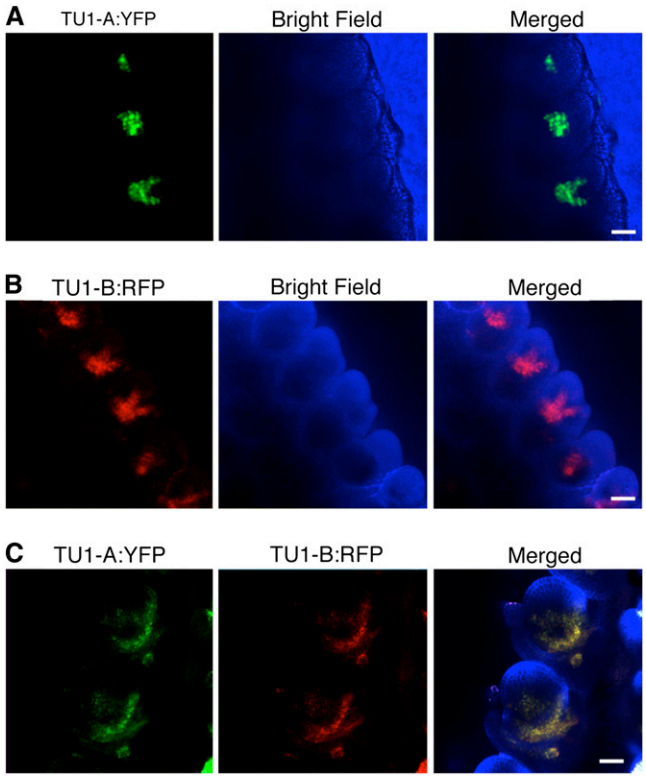

Figure 8. Developmental Expression of TU1-A:YFP and TU1-B:RFP in Immature Ears.

(A) and **(B)** In 2-mm ears, TU1-A:YFP **(A)** and TU1-B:RFP **(B)** are expressed at specific cup-shaped domains subtending SPM, respectively. Bright field images in **(A)** and **(B)** were converted into blue channel for better contrast.
(C) Transgenic plants harboring both *Tu1-A:YFP* and *Tu1-B:RFP* showed colocalization of TU1-A:YFP and TU1-B:RFP at the base of the SM in ~4-mm-long ears.
Bars in **(A)** to **(C)** = 20 μm.

(Hartmann et al., 2000), whereas the closely related *AGAMOUS-LIKE24* (*AGL24*) regulates FM identity and causes floral reversion with bract-like sepals and no petals when overexpressed (Yu et al., 2004). In rice (*Oryza sativa*), the ectopic expression of Os-*MADS22*, the *Zmm19* ortholog, causes abnormal floral morphology, including loss of the palea from spikelets, elongated glumes, and a two-floret spikelet, a mild form of SM indeterminacy (Sentoku et al., 2005). In barley (*Hordeum vulgare*), the *Zmm19* homolog *MADS1* (*BM1*) is expressed in vegetative tissues and repressed during floral development and also induces floral reversion by repressing spike development when ectopically expressed (Trevaskis et al., 2007). Thus, the molecular role of *Zmm19* orthologs is at least partially conserved in other species. MADS domain proteins bind CArG box *cis*-regulatory elements (Pollock and Treisman, 1991; Shore and Sharrocks, 1995), and these are present in 5′ upstream regions of *Ra1*, *Ra2*, *Ra3*, *Ts1*, *Ts2*, and *Ts4*, all of which interact with *Tu1*. It is plausible that ZMM19 may recognize these binding sites and contribute to pleiotropic alterations in inflorescence architecture that are exacerbated in double mutants. In addition to dramatically enhanced glume length, homozygous plants with four copies of the gene fusion have branch determination defects resembling *ramosa* mutants. These defects are consistent with the idea that *Ramosa1* and *Tu1* activity may be mutually repressive, via the coincidence of the expression patterns of *Ra1*, *Ra3*, and *Tu1*. Both *ra1* and *Tu1* mutants were first considered to be distinct subspecies, and Collins (1917) described hybrids of *Zea ramosa* and *Zea tunicata* (*ra1*/*ra1 Tu1*/+) as sterile highly branched cauliflower-like inflorescences (Langdale et al., 1994). This "monstrous" phenotype (Collins, 1917) presumably reflects the coexpression described here.

Mangelsdorf famously proposed that a half-tunicate form of *Tu1* was present in the teosinte ancestors of maize but was only revealed phenotypically in crosses to the Mexican popcorn, *Palomero toluqueño* (Mangelsdorf, 1974). Several inbred accessions of teosinte have recently been sequenced, as well as the Mexican popcorn (Chia et al., 2012). We searched for the junctions of the 1.8-Mb inversion in these genomic sequences and found no evidence for the existence of this gene fusion, although the sequences on either side were intact. Although we cannot exclude the possibility that additional accessions of teosinte may have the rearrangement, our results are consistent with a single late origin for *Tu1*, after the domestication of maize.

METHODS

Plant Material

The *Tu1* (number 412G), *Tu1-l* (number 416B), and *Tu1-md* (number 416E) alleles in an unknown genetic background were obtained from the Maize Genetics Coop Stock Center. *Tu1*, *Tu1-l*, and *Tu1-md* plants were introgressed into B73 two times. B73 was used as the wild-type line. Plants were grown in the field or in the green house under standard conditions.

Fine Mapping

Heterozygous *Tu1* plants were crossed to the B73 inbred line, and then F1 heterozygous *Tu1* plants were backcrossed to B73 to generate mapping populations segregating equally for wild-type and mutant at a 1:1 ratio. Phenotypes of ~750 F2 plants were scored by visual inspection of mature tassels and ears. DNA preps were done on 738 plants for positional cloning. SSR and IDP markers were used on chromosome 4L, where the *Tu1* locus is located, as previously described (Mangelsdorf and Galinat, 1964). The F2 population was screened with markers IDP8954 and umc2009 on chromosome 4L to identify recombinants. To narrow the mapping interval, CAPS (Konieczny and Ausubel, 1993) and InDel markers were designed for maize (*Zea mays*) genes by sequencing and identifying sequence polymorphisms between B73 and the *Tu1* progenitor. Genetic markers were amplified with 20 to 60 ng of DNA and Phusion High-Fidelity DNA polymerase (Finnzymes) by PCR using primers listed in Supplemental Table 1 online. SSR and IDP markers were tested according to the recommended PCR conditions (http://www.maizegdb.org/documentation/maizemap/ssr_protocols.php and magi.plantgenomics.iastate.edu/browseMarker.do, respectively). As a CAPS marker, GRMZM2G386088 PCR product was subsequently treated with the KpnI restriction enzyme at 37°C for 1 h and analyzed via 1% agarose gel electrophoresis.

Scanning Electron Microscopy

As described in Whipple et al. (2010), fresh samples of maize immature ears were dissected and mounted on disks with silver adhesive (Electron Microscopy Sciences) and placed on ice before imaging. A Hitachi S-3500N scanning electron microscope was used to capture images of the live sample by the electron beam using an accelerating voltage of 5.0 kV under high vacuum mode and a distance of 15 to 30 mm within 15 min.

Tu1-A:*YFP* and *Tu1-B*:*RFP* Transgenic Maize Lines

Tu1-A:*YFP* and *Tu1-B*:*RFP* transgenes were constructed by cloning *Tu1-A* and *Tu1-B* alleles, respectively, using homozygous *Tu1* DNA. *Tu1-A*:*YFP* construct was generated by fusing YFP in-frame to the C terminus before the stop codon of the genomic sequence of *Tu1-A*, including 700 bp of the 3′ downstream region of GRMZM2G006297, 2 kb of the *Mu-like* element, 300 bp of the 5′ promoter, a complete *Tu1-A* coding sequence with a 3.5-kb insertion in the first intron, and 450 bp of the 3′ untranslated region (UTR). The MultiSite Gateway Four Fragment System (Invitrogen) was used, by modifying the method described in Mohanty et al. (2009). All fragments were amplified using Phusion *Taq* polymerase (Finnzymes). The first fragment from the 5′ upstream region to the 3.5-kb insertion within the first intron was amplified with primers *Tu1*AB_attB1 and *Tu1*A_attB5(R) and cloned into the pDONR221 P1-P5R vector using BP recombinase (Invitrogen). The second fragment from the remaining first intron to the coding sequence before the stop codon was amplified with primers *Tu1*A_attB5 and *Tu1*AB_attB4 and cloned into the pDONR221 P5-P4 vector. The citrine YFP fragment was amplified with primers YFP_attB4(R) and YFP_attB3(R) and cloned into the pDONR221 P4r-P3r vector using BP recombinase (Invitrogen). The third fragment from the stop codon to the 3′ UTR was amplified with primers *Tu1*AB_attB3 and *Tu1*AB_attB2 and cloned into the pDONR221 P3-P2 vector. The pDONR221 P1-P5R, pDONR221 P5-P4, pDONR221 P4r-P3r, and pDONR221 P3-P2 vector fragments were combined and transferred to the pTF101 Gateway-compatible maize transformation vector by a multisite LR recombination reaction (Invitrogen). Confirmed clones were transferred to *Agrobacterium tumefaciens* and transformed into maize (Mohanty et al., 2009). The same protocol was applied for the *Tu1-B*:*RFP* construction. For the *Tu1-B*:*RFP* construct, *Tu1*B_attB5(R) and *Tu1*-B_attB5 primers were used to amplify the first and second fragment specific to *Tu1*-B. The mRFP1 fragment was amplified with primer RFP_attB4(R) and RFP_attB3(R) and cloned into the pDONR221 P4r-P3r vector. The same third fragment was used, because the 3′ UTR is identical between *Tu1-A* and *Tu1-B*. Likewise, four vector fragments were combined and transferred to the pTF101 vector. Confirmed clones were

transferred to *Agrobacterium* and were transformed into maize. The sequences of the primers are shown in Supplemental Table 2 online.

Allele-Specific Long-Range PCRs and Sequencing

For all PCR reactions, genomic DNA was extracted from wild-type inbred lines and plants homozygous for *Tu1* mutations. PCR amplification of *Tu1* alleles was performed with Phusion High-Fidelity DNA polymerase (Finnzymes) and allele-specific primers (see Supplemental Table 3 online) under optimal PCR conditions, according to Finnzymes's recommendations. For the long-range PCRs, TaKaRa LA *Taq* polymerase was used with primers (see Supplemental Table 3 online) under two-step PCR conditions following the provided protocol. The PCR product was subsequently prepared for Illumina DNA sequencing according to the manufacturer's recommendations. Sequencing was performed on an Illumina Genome Analyzer "GAII" for PE50 cycles.

qRT-PCR

Total RNA was extracted from immature tassels (1 to 2 cm long) and immature ears (0.5 to 0.9 cm long) using TRIzol reagent (Invitrogen). Total RNA was treated with DNaseI and reverse transcribed using an oligo-dT primer and SuperScript III Reverse Transcriptase (Invitrogen). qRT-PCR was performed with iQ SYBR Green Supermix (Bio-Rad) using two technical replicates each of two or three biological replicates. qRT-PCR primers are listed in Supplemental Table 1 online. qRT-PCR reactions were annealed at 57°C. The relative expression values for all experiments were calculated based on the expression of the experimentally validated control gene *Ubiquitin* as previously described (Satoh-Nagasawa et al., 2006). qRT-PCR was performed on a CFX96 thermocycler, and the results were analyzed on the CFX Manager Software package (Bio-Rad). Relative expression was calculated using the delta-delta method equation $2^{-[\Delta CP\ sample\ -\ \Delta CP\ control]}$, where 2 represents perfect PCR efficiency.

Confocal Microscopy

Inflorescences in different developmental stages were hand-sectioned and visualized in water. Immature ears were counterstained with Calcoflour for 2 min and washed with a buffer (50% glycerol, 1× PBS, and 0.1% NaAzide). Fluorescent proteins were detected on an LSM 710 confocal microscope (Carl Zeiss). Bright field images were collected together with fluorescence images using the transmitted light detector and were processed into a blue background using Zeiss ZEN software and Adobe Photoshop CS4.

Accession Numbers

Sequence data from this article can be found in the GenBank and MaizeSequence (MaizeSequence.org) databases under the following accession numbers: *Tu1-A* (AJ850302), *Tu1-B* (AJ850303), *Tu1-d* (AJ850299), *Tu1-l* (AJ850300), and *Tu1-md* (AJ850301), GRMZM2G370777, and GRMZM2G006297.

Supplemental Data

The following materials are available in the online version of this article.

Supplemental Figure 1. Half-Tunicate Phenotype of Single Copy *Tu1-md* and *Tu1-rec* Heterozygous Mutants.

Supplemental Figure 2. A 30-kb Tandem Duplication at *Tu1*.

Supplemental Figure 3. Upregulation of *Zmm19* Expression in *Tu1* Reproductive Tissues.

Supplemental Figure 4. *Tu1-A*:*YFP* and *Tu1-B*:*RFP* Transgenic Tassels Phenocopy *Tu1* in a Dose-Dependent Manner.

Supplemental Figure 5. TU1-A:YFP Is Expressed in Vegetative and Reproductive Tissues.

Supplemental Figure 6. TU1-A:YFP and TU1-B:RFP Proteins Are Colocalized in Nuclei.

Supplemental Figure 7. Gene Expression Data of GRMZM2G370777 and GRMZM2G006297.

Supplemental Table 1. Primers Used in Fine-Mapping and qRT-PCR.

Supplemental Table 2. Primers Used in Transgene Construction.

Supplemental Table 3. Primers Used in Allele-Specific and Long-Range PCRs.

ACKNOWLEDGMENTS

We thank Jer-Ming Chia and Doreen Ware for sharing sequence information and Sarah Hake for sharing KN1 chromatin immunoprecipitation sequencing data before publication. We thank Tim Mulligan for expert farm care and Peter Bommert and Alexander Goldshmidt for advice with mapping and microscopy. We also thank Andrea Eveland and Alexander Goldshmidt for sharing RNA sequencing data before publication and Evan Ernst for assembling DNA sequence reads. This study is in partial completion of a PhD degree at Stony Brook University, and Jong-Jin Han thanks his thesis committee members, David Jackson, Tom Brutnell, Alea Mills, and Vitaly Citovsky for their advice and support. We thank Guenter Theissen and colleagues for depositing the sequence of *Zmm19* from *Tu1* in GenBank in 2004. While our article was in preparation, these sequences were hypothesized to contribute to the pod corn phenotype and appeared online in advance of publication (Wingen et al., 2012). This study was supported by grants from the National Science Foundation to R.M. (DBI-0527192) and D.J. (MCB-1027445).

AUTHOR CONTRIBUTIONS

J.-J.H. performed the experiments, D.J. provided advice, materials, and help with microscopy, and R.M., D.J., and J.-J.H. designed the experiments and wrote the article.

Received May 17, 2012; revised June 21, 2012; accepted July 6, 2012; published July 24, 2012.

REFERENCES

Aukerman, M.J., and Sakai, H. (2003). Regulation of flowering time and floral organ identity by a MicroRNA and its APETALA2-like target genes. Plant Cell **15:** 2730–2741.

Bolduc, N., and Hake, S. (2009). The maize transcription factor KNOTTED1 directly regulates the gibberellin catabolism gene ga2ox1. Plant Cell **21:** 1647–1658.

Bolduc, N., Yilmaz, A., Mejia-Guerra, M.K., Morohashi, K., O'Connor, D., Grotewold, E., and Hake, S. (2012). Unraveling the KNOTTED1 regulatory network in maize meristems. Genes Dev. **26:** 1685–1690.

Bortiri, E., Chuck, G., Vollbrecht, E., Rocheford, T., Martienssen, R., and Hake, S. (2006). ramosa2 encodes a LATERAL ORGAN BOUNDARY domain protein that determines the fate of stem cells in branch meristems of maize. Plant Cell **18:** 574–585.

Bortiri, E., and Hake, S. (2007). Flowering and determinacy in maize. J. Exp. Bot. **58:** 909–916.

Chen, X. (2004). A microRNA as a translational repressor of APETALA2 in *Arabidopsis* flower development. Science **303:** 2022–2025.

Chia, J.-M., et al. (2012). Maize HapMap2 identifies extant variation from a genome in flux. Nat. Genet. **44:** 803–807.

Chuck, G., Cigan, A.M., Saeteurn, K., and Hake, S. (2007a). The heterochronic maize mutant Corngrass1 results from overexpression of a tandem microRNA. Nat. Genet. **39:** 544–549.

Chuck, G., Meeley, R., Irish, E., Sakai, H., and Hake, S. (2007b). The maize tasselseed4 microRNA controls sex determination and meristem cell fate by targeting Tasselseed6/indeterminate spikelet1. Nat. Genet. **39:** 1517–1521.

Collins, G.N. (1917). Hybrids of *Zea tunicata* and *Zea ramosa*. Proc. Natl. Acad. Sci. USA **3:** 345–349.

Eyster, W.H. (1921). The linkage relations between the factors for tunicate ear and starchy-sugary endosperm in maize. Genetics **6:** 209–240.

Hartmann, U., Höhmann, S., Nettesheim, K., Wisman, E., Saedler, H., and Huijser, P. (2000). Molecular cloning of SVP: A negative regulator of the floral transition in *Arabidopsis*. Plant J. **21:** 351–360.

Hartwig, T., Chuck, G.S., Fujioka, S., Klempien, A., Weizbauer, R., Potluri, D.P., Choe, S., Johal, G.S., and Schulz, B. (2011). Brassinosteroid control of sex determination in maize. Proc. Natl. Acad. Sci. USA **108:** 19814–19819.

He, C., Münster, T., and Saedler, H. (2004). On the origin of floral morphological novelties. FEBS Lett. **567:** 147–151.

Konieczny, A., and Ausubel, F.M. (1993). A procedure for mapping *Arabidopsis* mutations using co-dominant ecotype-specific PCR-based markers. Plant J. **4:** 403–410.

Langdale, J.A., Irish, E.E., and Nelson, T.M. (1994). Action of the tunicate locus on maize floral development. Dev. Genet. **15:** 176–187.

Le Roux, L.G., and Kellogg, E.A. (1999). Floral development and the formation of unisexual spikelets in the Andropogoneae (Poaceae). Am. J. Bot. **86:** 354–366.

Mangelsdorf, P.C. (1947). The origin and evolution of maize. Adv. Genet. **1:** 161–207.

Mangelsdorf, P.C. (1974). Corn: Its Origin, Evolution and Improvement. (Cambridge, MA: Harvard University Press).

Mangelsdorf, P.C. (1984). The origin of maize. Science **225:** 1094.

Mangelsdorf, P.C., and Galinat, W.C. (1964). The tunicate locus in maize dissected and reconstituted. Proc. Natl. Acad. Sci. USA **51:** 147–150.

Mangelsdorf, P.C., Macneish, R.S., and Galinat, W.C. (1964). Domestication of corn. Science **143:** 538–545.

Mohanty, A., Luo, A., DeBlasio, S., Ling, X., Yang, Y., Tuthill, D.E., Williams, K.E., Hill, D., Zadrozny, T., Chan, A., Sylvester, A.W., and Jackson, D. (2009). Advancing cell biology and functional genomics in maize using fluorescent protein-tagged lines. Plant Physiol. **149:** 601–605.

Münster, T., Deleu, W., Wingen, L.U., Ouzunova, M., Cacharron, J., Faigl, W., Wert, S., Kim, J.T.T., Saedler, H., and Theissen, G. (2002). Maize MADS-box genes galore. Maydica **47:** 287–301.

Munster, T., Wingen, L., Faigl, W., Deleu, W., Ahlbory, D., Sommer, H., Saedler, H., and Theissen, G. (2004). Pod corn (Tunicate maize) caused by the ectopic expression of a vegetative MADS-box gene in the inflorescence of maize. Genbank AJ850299–AJ850303.

Ng, M., and Yanofsky, M.F. (2001). Function and evolution of the plant MADS-box gene family. Nat. Rev. Genet. **2:** 186–195.

Nickerson, N.H., and Dale, E.E. (1955). Tassel modifications in *Zea mays*. Ann. Mo. Bot. Gard. **42:** 195–211.

Pollock, R., and Treisman, R. (1991). Human SRF-related proteins: DNA-binding properties and potential regulatory targets. Genes Dev. **5:** 2327–2341.

Saint-Hilaire, A. (1829). Lettre sur une variete remarquable de Mais du Bresil. Ann. Sci. Nat. **16:** 143–145.

Satoh-Nagasawa, N., Nagasawa, N., Malcomber, S., Sakai, H., and Jackson, D. (2006). A trehalose metabolic enzyme controls inflorescence architecture in maize. Nature **441:** 227–230.

Schnable, P.S., et al. (2009). The B73 maize genome: Complexity, diversity, and dynamics. Science **326:** 1112–1115.

Sentoku, N., Kato, H., Kitano, H., and Imai, R. (2005). OsMADS22, an STMADS11-like MADS-box gene of rice, is expressed in non-vegetative tissues and its ectopic expression induces spikelet meristem indeterminacy. Mol. Genet. Genomics **273:** 1–9.

Shore, P., and Sharrocks, A.D. (1995). The MADS-box family of transcription factors. Eur. J. Biochem. **229:** 1–13.

Trevaskis, B., Tadege, M., Hemming, M.N., Peacock, W.J., Dennis, E.S., and Sheldon, C. (2007). Short vegetative phase-like MADS-box genes inhibit floral meristem identity in barley. Plant Physiol. **143:** 225–235.

Vollbrecht, E., Springer, P.S., Goh, L., Buckler IV, E.S., and Martienssen, R. (2005). Architecture of floral branch systems in maize and related grasses. Nature **436:** 1119–1126.

Wei, F., et al. (2009). Detailed analysis of a contiguous 22-Mb region of the maize genome. PLoS Genet. **5:** e1000728.

Whipple, C.J., Ciceri, P., Padilla, C.M., Ambrose, B.A., Bandong, S.L., and Schmidt, R.J. (2004). Conservation of B-class floral homeotic gene function between maize and *Arabidopsis*. Development **131:** 6083–6091.

Whipple, C.J., Hall, D.H., DeBlasio, S., Taguchi-Shiobara, F., Schmidt, R.J., and Jackson, D.P. (2010). A conserved mechanism of bract suppression in the grass family. Plant Cell **22:** 565–578.

Wingen, L.U., Münster, T., Faigl, W., Deleu, W., Sommer, H., Saedler, H., and Theißen, G. (2012). Molecular genetic basis of pod corn (*Tunicate* maize). Proc. Natl. Acad. Sci. USA **109:** 7115–7120.

Yu, H., Ito, T., Wellmer, F., and Meyerowitz, E.M. (2004). Repression of AGAMOUS-LIKE 24 is a crucial step in promoting flower development. Nat. Genet. **36:** 157–161.

Yu, H., Xu, Y., Tan, E.L., and Kumar, P.P. (2002). AGAMOUS-LIKE 24, a dosage-dependent mediator of the flowering signals. Proc. Natl. Acad. Sci. USA **99:** 16336–16341.

Zhu, Q.H., and Helliwell, C.A. (2011). Regulation of flowering time and floral patterning by miR172. J. Exp. Bot. **62:** 487–495.